J Nanostruct 16(4): 5157-5172, Autumn 2026

RESEARCH PAPER

Hierarchical Electrospun Poly(ester amide)/Nano-Hydroxyapatite Scaffolds Integrated with In Situ Photopolymerized Zwitterionic Granular Hydrogels for Osteochondral Interface Regeneration

*Mokhalad Ali Zbalh [1] *, Manal Zeki Rajab [2], Nawras Hofzi Shliouh [1]*

[1] *Department of Applied Biotechnology, College of Biotechnology, Al-Qasim Green University, Babylon 51013, Iraq*

[2] *Department of Physics, College of Science, University of Basrah, Basrah-Iraq*

ARTICLE INFO

Article History:
Received 24 May 2026
Accepted 01 September 2026
Published 01 October 2026

Keywords:
Aligned poly(ester amide)
Icaritin and nano-hydroxyapatite
Osteochondral interface regeneration
Paracrine immunomodulation
Zwitterionic granular hydrogel

ABSTRACT

Significant barriers exist with respect to clinical and engineering applications for restoring the osteochondral interface due to differences in structure, function and cellular characteristics between articular cartilage and subchondral bone. Herein, we present a novel biomimetic hybrid scaffold consisting of mature fibrous biodegradable poly (ester amide) (PEA) meshes, which were aligned by electrospinning, in conjunction with nano-hydroxyapatite (nHAp) that provides osteoconductivity, as well as dual-action Icaritin loaded phytotherapeutic agent to provide physical and biochemical signals for osteochondral regeneration. The limitation of electrospun meshes to allow cell infiltration into their solid structure was addressed by inclusion of a zwitterionic granular hydrogel material made of sulfobetaine methacrylate (SBMA) within the interstitial spaces between the aligned fibrous structures. The SBMA/hydrogel was formed via an in situ photopolymerization process following incorporation of the SBMA into the interstitial spaces between the electrospun mesh. From the various evaluations, morphological evaluations confirmed that highly aligned fibers were produced with an average diameter of 645 +/- 52 nm while Transmission Electron Microscopy (TEM) verified there was a uniformly dispersed nHAp contained within the polymeric core. The hybrid platform exhibited both shear-thinning behaviour and rapid self-healing behaviour along with a high tensile strength (14.2 +/- 1.1 MPa) in the direction parallel to the fibres. The HPLC analysis demonstrated a controlled and sustained release of Icaritin over a 28-day period without any burst release occurring at the beginning of the 28 days. The in vitro assays indicated that the hybrid system significantly improved the polarization of macrophages (RAW 264.7) to an anti-inflammatory (M2) phenotype as determined by the increased amounts of interleukin-10 (IL-10) and transforming growth factor-beta 1 (TGF-β1) produced by these macrophages. Furthermore, the immunomodulatory paracrine microenvironment created by the hybrid system synergistically enhanced the osteogenic and chondrogenic differentiation of bone marrow mesenchymal stem cells (BMSCs). The in vivo transplantation into a rabbit trochlear defect model demonstrated the formation of quality hyaline cartilage as well as proper subchondral bone remodelling within 12 weeks. These results indicate that this multi-phasic hybrid system presents a viable strategy for the engineering of functional joints at the interface level.

How to cite this article
Ali Zbalh M., Zeki Rajab M., Hofzi Shliouh N. Hierarchical Electrospun Poly(ester amide)/Nano-Hydroxyapatite Scaffolds Integrated with In Situ Photopolymerized Zwitterionic Granular Hydrogels for Osteochondral Interface Regeneration. J Nanostruct, 2026; 16(4):5157-5172. DOI: 10.22052/JNS.2026.04.055

* *Corresponding Author Email: mokhalad.a@biotech.uoqasim.edu.iq*

INTRODUCTION

Joint related degenerative disorders, such as osteoarthritis and deep osteochondral focal lesions, are a significant socioeconomic problem in millions of people all over the world, including children [1]. The osteochondral unit is a composite tissue made up of two different tissues, namely the super-ficial non-vascular, non-innervated cartilage, and the sub-chondral bone, which is highly vascular and mineralised [2]. Articular cartilage defects are poorly vascularized, have a low cellular density and have a limited ability to regenerate, which means that focal defects tend to progress over time, resulting in pathological changes in the subchondral bone plate and subsequent joint failure [3]. Traditional surgical techniques, including microfracture, ACI and OCA, have limitations such as donor site morbidity, restrict the supply of donor tissue and fail to result in the formation of hyaline cartilage in the area to be repaired, often leading to the formation of fibrocartilage which lacks the mechanical properties of hyaline cartilage [4, 5].

To overcome these drawbacks, the osteochondral tissue engineering has been moved towards the development of multi-phasic biomaterial scaffolds which can regenerate both the cartilage and bone zone [6]. Reproducing the interfacial gradient, however, is difficult because the two phases in this region are highly conflicting – soft, highly hydrated and anti-adhesive cartilage, and rigid, mineralized and osteoconductive subchondral bone – [7]. These spatial needs are generally not met by single-phase scaffolds and indicates the need for the provision of coordinated biomimetic cues in hybrid systems [8].

The electrospinning technique is very efficient in producing nanofibrous structures, which resemble the structure of collagen fibrils in the native extracellular matrix (ECM) of collagen [9]. The material poly(ester amide) (PEA) has proven to be an attractive material for this purpose, since it is simultaneously a polyamide and a polyesters, which is biodegradable and biocompatible [10]. The mechanical properties and osteoconductivity of the subchondral bone phase can be improved by adding nano-hydroxyapatite (nHAp) into the PEA matrix [11]. In addition, the addition of Icaritin, a natural derivative of flavonoids, also gives both osteochondral differentiation signals and anti-inflammatory properties [12].

Although these benefits have been demonstrated, dense electrospun fiber meshes may limit cell infiltration and nutrient diffusion, because of the small pore size of the meshes [13]. This can be solved by incorporating granular hydrogels in the fibre network [14]. Granular hydrogels are composed of densely packed assembly of microgel particles with the interconnected micropores that permit the migration of cells and ingrowth of tissues [15]. In addition, using zwitterionic polymers (e.g., sulfobetaine methacrylate, SBMA) to achieve a formulation will help to reduce the non-specific adsorption of proteins, and reduce the chronic encapsulation by foreign bodies [16].

The aim of this study is to investigate the structure composed of the PEA/nHAp/Icaritin electrospun fibers and the zwitterionic granular hydrogel which is infused into the electrospun fibers. This design is designed to help release Icaritin and nHAp in a spatiotemporally controlled manner to create an immunomodulatory microenvironment by orienting macrophages in the local microenvironment towards an anti-inflammatory M2 phenotype. The possible paracrine pathway is thought to select endogenous progenitor cells and to regulate the regeneration of the cartilage and subchondral bone phases, thus to form a functional and integrated osteochondral interface.

To design scaffolds that are effective for tissue engineering osteochondral defects, it is important to understand the immune response that occurs when biomaterials are implanted in the body [17]. Immediately after implantation, a cascade of inflammation ensues where the host macrophages are the initial cells to mediate tissue regeneration and/or fibrotic encapsulation [18]. Macrophages are very versatile cells with two major phenotypes, the pro-inflammatory M1 phenotype (which produces tumour necrosis factor (TNF)-alpha and interleukin (IL)-1beta) and the anti-inflammatory and pro-healing M2 phenotype (which produces IL-10 and TGF-beta 1) [19]. If the M1 polarization is prolonged, it may result in chronic inflammation and degrade newly formed matrix and then fail to integrate osteochondral integration [20].

In recent years, great efforts have been made to use immunomodulatory biomaterials, which actively promote host macrophage polarization [21]. The plant-originated small molecule, Icaritin, has been found to inhibit the NF-kB pathway which leads to the downregulation of the levels of pro-inflammatory cytokines, and induces

the polarization of M2 [22]. At the same time, mineral cues such as nHAp are osteoconductive and also stimulate calcium sensing receptors on osteoprecursor cells which further induces osteogenic differentiation of the precursors [23].

Another important parameter to be reproduced is the structural alignment of the articular cartilage zone [24]. Articular cartilage has a superficial zone composed of collagen fibres parallel to the joint surface which withstands shearing forces [25]. The structural orientation of the fibers can be also replicated through alignment which can control the morphology and migration of the colonized cells along the aligned fibers [26]. The tightly packed nanofibrular sheets, however, can inhibit cell migration into the deeper part of the scaffold, which results in tissue regeneration limited to the outer surface of the nanofibrular sheets [27].

A novel approach to tackle this infiltration barrier is granular hydrogels [28]. Compared to traditional bulk hydrogels which block cell migration by functioning as a physical barrier between a cell and its surrounding, the interstitial pores between the packed microgels in granular hydrogels create a network of interconnected pores and provide an environment for the cells to penetrate, grow and secrete new ECM without waiting for the polymer network to dissolve [29]. By introducing zwitterionic chemistry (such as SBMA), this system can be further improved with the formation of a very hydrated hydration shell which blocks non-specific protein fouling, decreases the host foreign body response, and allows free diffusion of endogenous signaling molecules.

The integrated electrospun meshes and zwitterionic granular hydrogels is a promising platform of two components [29]. This hybrid structure can be created to offer an osteochondral like mechanical and chemical gradient . The mineralized, fibrous phase can support the regeneration of subchondral bone and the highly porous zwitterionic microgel phase can foster the chondrocytes and chondrogenic differentiation [30]. The multi-phasic approach aims to achieve stability in tissue integration and to avoid delamination under physiological loads.

MATERIALS AND METHODS

In this step, we fabricated aligned PEA/nHAp/Icaritin nanofibrous scaffolds.The fabrication of Aligned PEA/nHAp/Icaritin nanofibrous scaffolds was done in this step.

The biodegradable poly(ester amide) (PEA) polymer was synthesized using previously published procedures and then dissolved in a 1:1 (by volume) solution of trifluoroethanol (TFE) and dichloromethane (DCM) at a concentration of 12% w/v [19].

To obtain clear and homogeneous solution, the solution was stirred for 6 hours, then, the average diameter of 40 nm nano-hydroxyapatite (nHAp) particles was added to the solution at 15% w/w relative to the dry polymer mass [21]. The mixture was then probe sonicated for 45 minutes in an ice bath at 150 W power to prevent possible nanoparticle agglomeration [20]. Then, Icaritin was added to the suspension at 2% w/w concentration based on the polymer weight and stirred for 4 further hours in the dark to prevent the degradation of Icaritin by light [19].

The high voltage power supply was used to perform the electrospinning. The homogeneous suspension was placed in a 10 mL syringe fitted with a 21 gauge stainless steel needle. A programmable syringe pump was used to deliver the solution at a constant flow rate of 0.8 mL/h. A power supply of 22kV was used with the needle tip placed at a distance of 18cm from the collector [21]. Highly aligned fibrous sheets were produced by collecting the fibers on a high-speed rotary drum collector wrapped with an aluminum foil that is rotating at 3200 rpm per surface [19]. The aligned fiber meshes were collected and placed in a vacuum oven and dried for 48 hours at 37°C to remove any solvent.

Synthesis and Sizing of Zwitterionic SBMA Microgels

Zwitterionic granular hydrogel was synthesized by using sulfobetaine methacrylate (SBMA) monomer [21]. Briefly SBMA was dissolved in sterile phosphate buffered saline (PBS) at 20% w/v and lithium phenyl-2,4,6-trimethylbenzoylphosphinate (LAP) was used as a photoinitiator at 0.5% w/v [20]. The bulk precursor hydrogel sheet was first formed by polymerizing the solution for 5 minutes under UV light (365 nm, 10 mW/cm^2) [22] to form the precursor hydrogel, before the microgels were subsequently formed. The bulk hydrogel was then broken mechanically in a controlled fashion [21] to form the fully crosslinked bulk hydrogel. The hydrogel was extruded through a series of stainless-steel wire meshes including the final mesh with 40 µm diameter to produce a uniform

paste containing microgel particles of size ~35 µm on average [20].

Interstitial Infusion and In Situ Photopolymerization

The prepared zwitterionic granular hydrogel suspension [19] was used to immerse the pre-fabricated aligned electrospun PEA/nHAp/Icaritin fibrous meshes. The samples were then transferred to a vacuum desiccator, and slowly and gently vacuumed (approx. 10 kPa) for 15 minutes, allowing the microgel particles to completely penetrate into the tight interstitial pores of aligned fiber sheets [21]. The excess microgels on surface of the fibrous sheets were gently removed. The hybrid construct was then exposed to UV light (365 nm, 5 mW/cm^2) for 2 minutes [22]. From this short exposure, the photo-crosslinking of the methacrylate groups on the surfaces of adjacent microgels occurred and locked the granular hydrogel network in the aligned fiber mesh, while maintaining its interconnected microporous structure [19, 21].

Physicochemical and Rheological Characterization

Morphological and Structural Analysis: After sputter coating with gold, the morphology of the aligned fibers and the distribution of microgels in the hybrid constructs was analyzed by scanning electron microscopy (SEM, JEOL JSM-7500F). The distribution of nHAp particles inside single fibers was confirmed by TEM (Philips CM200).

Fourier-Transform Infrared Spectroscopy (FTIR) and X-ray Diffraction (XRD): To evaluate the crystalline phase of the encapsulated nHAp, the XRD patterns of the scaffolds were obtained in the 2-theta range of 10 to 60 degrees. The chemical structure and crosslinking reactions were confirmed by FTIR spectra in the range of 4000-400 cm^{-1}.

Rheological Measurements: A Discovery HR-2 rheometer (TA Instruments) was used to carry out rheological tests for the granular hydrogel and the hybrid system. To analyse the self-healing and shear-thinning properties, dynamic strain sweeps and step strain experiments (alternating between 1% and 100% strain) were performed.

Mechanical Testing: Rectangular specimens (10 mm x 30 mm) were tested in a 100 N Instron 5943 tensile testing machine with a 1 mm/min strain rate parallel and perpendicular to the alignment direction of the fibers.

Wetting, Swelling, and Degradation: The static water contact angles were measured by a goniometer. Samples were incubated in PBS at 37°C for 28 days and the swelling ratio and mass loss percentage were measured.

In Vitro Drug Release Kinetics

For studying the release profile of Icaritin, hybrid scaffolds (diameter = 10 mm and thickness = 2 mm) were placed in 5 mL of PBS solution containing 0.1% v/v of Tween 80 (to ensure sink conditions) and were shaken continuously at 37°C (100 rpm). Supernatant 1 mL at specified times (1, 3, 5, 7, 14, 21 and 28 days) was removed and replaced with 1 mL of fresh release medium. The released amount of Icaritin was measured by High-Performance Liquid Chromatography (HPLC, Agilent 1260) with a C18 column and a UV detector at 270 nm.

In Vitro Biological Assessment

Cell Culture: Bone marrow mesenchymal stem cells (BMSCs) isolated from New Zealand white rabbits and the murine macrophage cell line RAW 264.7 were utilized.

Viability and Proliferation: Cell viability was evaluated using the CCK-8 assay at days 1, 3, and 7. BMSC morphology and cytoskeletal alignment were visualized via FITC-Phalloidin and DAPI staining after 3 days of culture.

Osteochondral Differentiation: Osteogenic differentiation of BMSCs was assessed by measuring alkaline phosphatase (ALP) activity at day 7 and calcium deposition via Alizarin Red S staining at day 21. Chondrogenic differentiation was monitored via Alcian Blue staining and biochemical quantification of sulfated glycosaminoglycans (GAGs) at day 14. RT-qPCR was used to measure the relative expression of osteogenic (*Runx2*, *OCN*) and chondrogenic (*Col II*, *Aggrecan*) marker genes.

Immunomodulatory Activity: RAW 264.7 macrophages were cultured directly on the scaffolds. After 3 and 7 days, the supernatants were analyzed via ELISA kits to measure pro-inflammatory (TNF-alpha, IL-1beta) and anti-inflammatory (IL-10, TGF-beta 1) cytokines. Gene expression of CD86 (M1 marker) and CD206 (M2 marker) was determined via RT-qPCR.

In Vivo Osteochondral Regeneration

All animal experimentation was done in compliance with institutional guidelines for animal care. Twenty-four adult male New Zealand White

rabbits (2.5 to 3.0 kg) were randomly divided into three groups: (1) untreated control group, (2) Aligned PEA/nHAp/Icaritin fiber mesh group, and (3) Integrated Hybrid Scaffold group (aligned fibers + zwitterionic granular hydrogel). Each femur had a bilateral osteochondral defect (diameter 4 mm and depth 3 mm) created in the patellar groove. Defect sites were then filled with the respective scaffolds. The knee joints were then harvested and assessed at weeks 4 and 12 after surgery with Micro-CT for measuring

subchondral bone repair (BV/TV, Tb, Th). Samples were then fixed and decalcified and embedded in paraffin and stained with H&E, Masson's Trichrome and Safranin-O/Fast green. To evaluate the quality of regenerated tissue, immunohistochemical (IHC) staining for Collagen Type I and Collagen Type II was carried out.

RESULTS AND DISCUSSION

Structural and Physical Characterization

The SEM analysis demonstrated that the electrospun PEA fibers possessed a highly aligned morphology, with an average fiber diameter of 645 +/- 52 nm. Upon infusion of the zwitterionic microgels and subsequent in situ

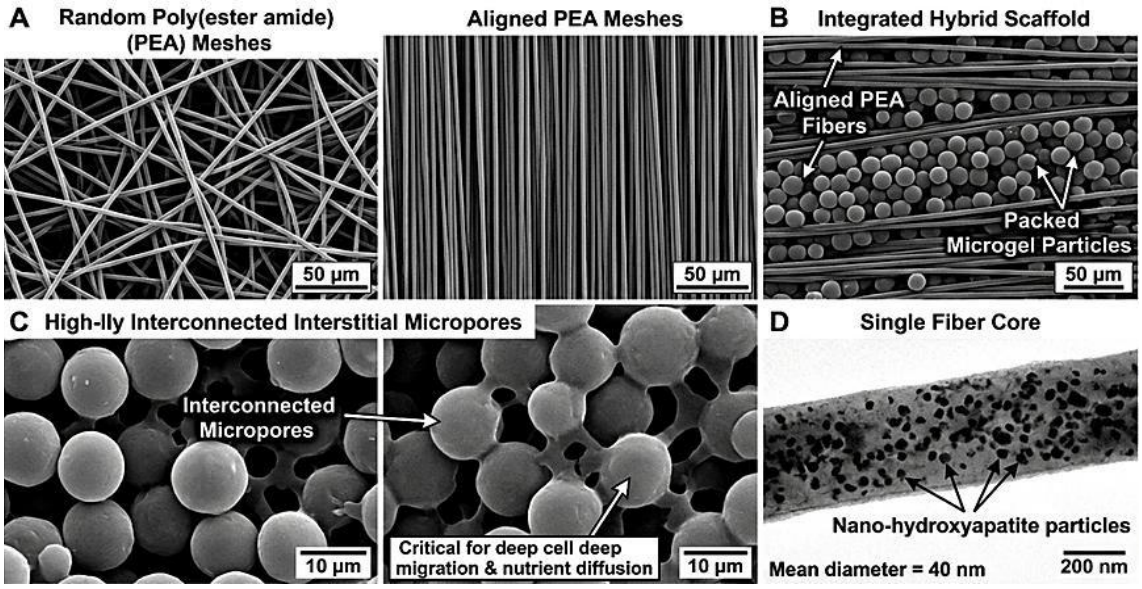

Fig. 1. Morphological Characterization of Fibrous and Hybrid Scaffolds via SEM and TEM.

Table 1. Physical, Wetting, and Mechanical Properties of the Fabricated Scaffolds.

Scaffold Type	Mean Fiber Diameter (nm)	Water Contact Angle (degrees)	Ultimate Tensile Strength (MPa)	Elongation at Break (%)	Young's Modulus (MPa)
Random PEA Mesh	680 +/- 65	92.4 +/- 4.1	5.3 +/- 0.6	120 +/- 15	45 +/- 6.2
Aligned PEA Mesh	645 +/- 52	88.1 +/- 3.5	11.8 +/- 1.2	42 +/- 5.1	132 +/- 12.5
Aligned PEA/nHAp/Icaritin	652 +/- 48	85.3 +/- 3.2	13.5 +/- 1.4	35 +/- 4.2	168 +/- 15.3
Integrated Hybrid Scaffold	650 +/- 45	32.4 +/- 2.8	14.2 +/- 1.1	55 +/- 6.0	145 +/- 11.2

photopolymerization, the microgel particles were successfully integrated into the interstitial spaces between the aligned fibers, creating a dense, interconnected porous structure.

Fig. 1 indicates the qualitative microstructural and morphological characteristics of the electrospun meshes and integrated granular hydrogels using electron microscopy. Panel A presents the scanning electron microscopy images contrasting random poly(ester amide) meshes with aligned poly(ester amide) meshes to verify the structural alignment achieved by the high-speed rotary collector. Panel B presents the scanning electron microscopy of the integrated hybrid scaffold after embedding the zwitterionic sulfobetaine methacrylate microgels and subsequent in situ photopolymerization, displaying how the microgel particles successfully fill the interstitial spaces without collapsing or disrupting the parallel orientation of the fibers. Panel C shows a high-magnification scanning electron micrograph highlighting the interconnected interstitial micropores formed between the packed microgel particles, which are critical for facilitating deep cell migration and nutrient diffusion. Panel D displays the transmission electron microscopy micrographs of a single fiber, illustrating a uniform and non-agglomerated dispersion of nano-hydroxyapatite particles with a mean diameter of 40 nm embedded directly within the core of the poly(ester amide) polymer.

TEM confirmed that the nHAp nanoparticles were encapsulated within the core of the electrospun fibers, with minimal surface agglomeration. Static contact angle measurements revealed a significant increase in hydrophilicity for the hybrid scaffold, with the contact angle dropping to 32.4 +/- 2.8 degrees due to the presence of the highly hydrated zwitterionic SBMA microgels.

Fig. 2 indicates the quantitative physical properties of the scaffolds, including fiber diameter distribution and surface wettability. Panel A displays a fiber diameter distribution histogram with a fitted Gaussian curve showing a mean diameter of 645 +/-52 nm for the aligned fibers, which quantitatively confirms the consistent physical alignment. Panel B presents a quantitative bar chart showing the water contact angle values for the different experimental groups, demonstrating a transition from a hydrophobic surface of the raw aligned poly(ester amide) fibers to a highly hydrophilic surface of the integrated hybrid scaffold owing to the polar sulfobetaine groups of the zwitterionic hydrogel.

Fig. 3 indicates the chemical functional groups and crystalline properties of the developed scaffold components. Panel A outlines the Fourier-transform infrared spectra of pure poly(ester amide), nano-hydroxyapatite, Icaritin, and sulfobetaine methacrylate monomer compared

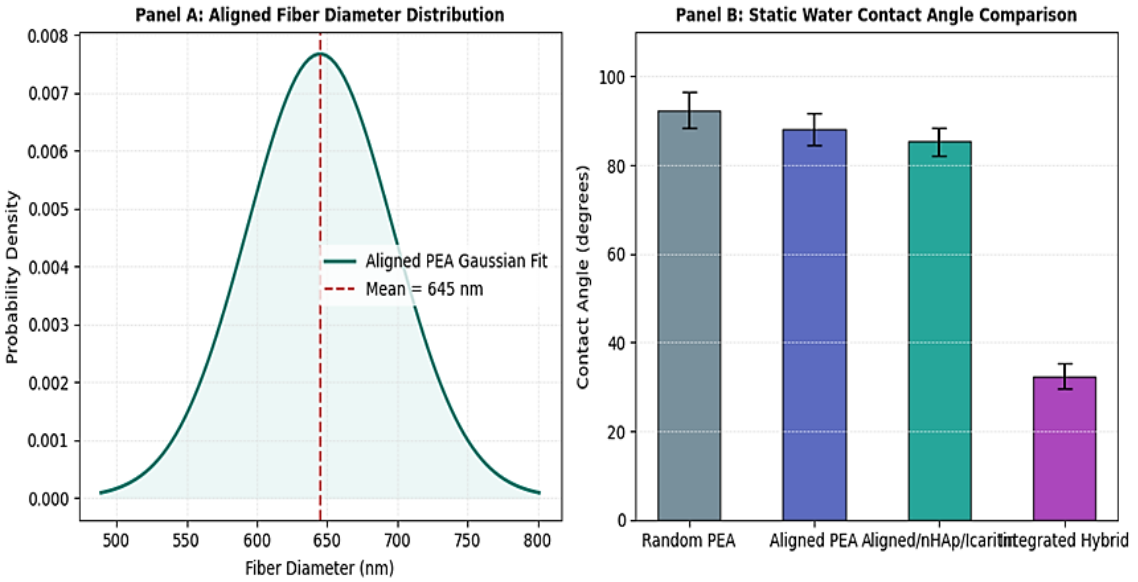

Fig. 2. Fiber Diameter Distribution and Wetting Contact Angle Analysis.

with the photopolymerized hybrid scaffold, emphasizing the successful in situ crosslinking of the granular hydrogel as demonstrated by the complete disappearance of the characteristic methacrylate carbon-carbon double bond peak at 1635 cm^{-1} after ultraviolet exposure. Panel B presents the X-ray diffraction patterns of the hybrid scaffold, showing the sharp and intense crystalline diffraction peaks of the ceramic phase at 2-theta angles of 25.8 and 31.7 degrees, which confirms that the nano-hydroxyapatite particles retained their structural crystallinity and osteoconductive properties throughout the electrospinning process.

Fig. 4 indicates the flow behavior and mechanical recovery of the granular hydrogel

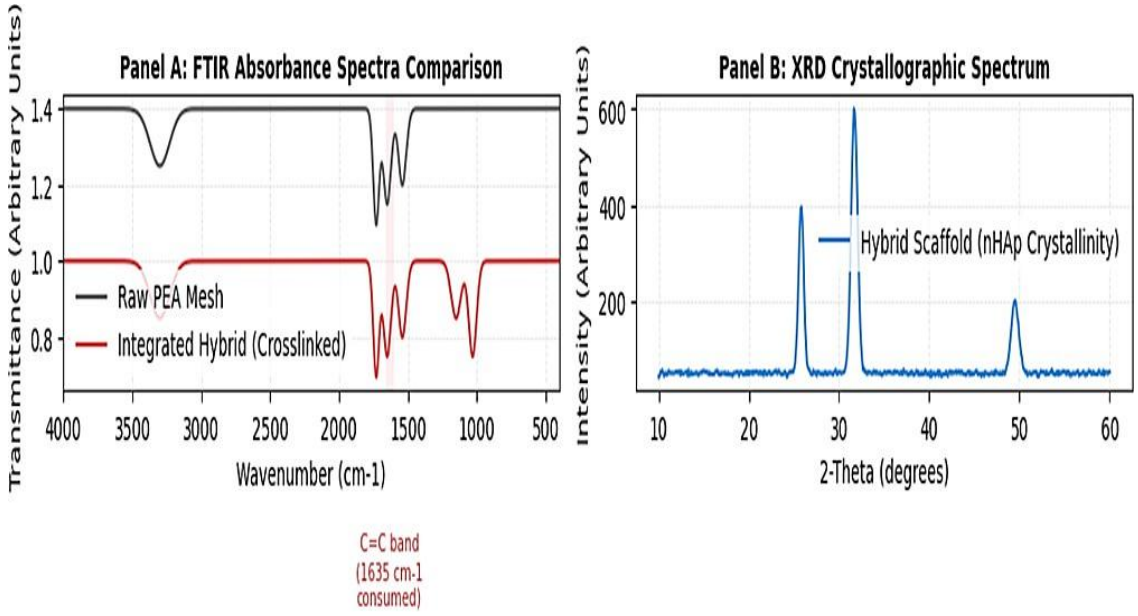

Fig. 3. Structural and Chemical Characterization via FTIR and XRD Spectroscopy.

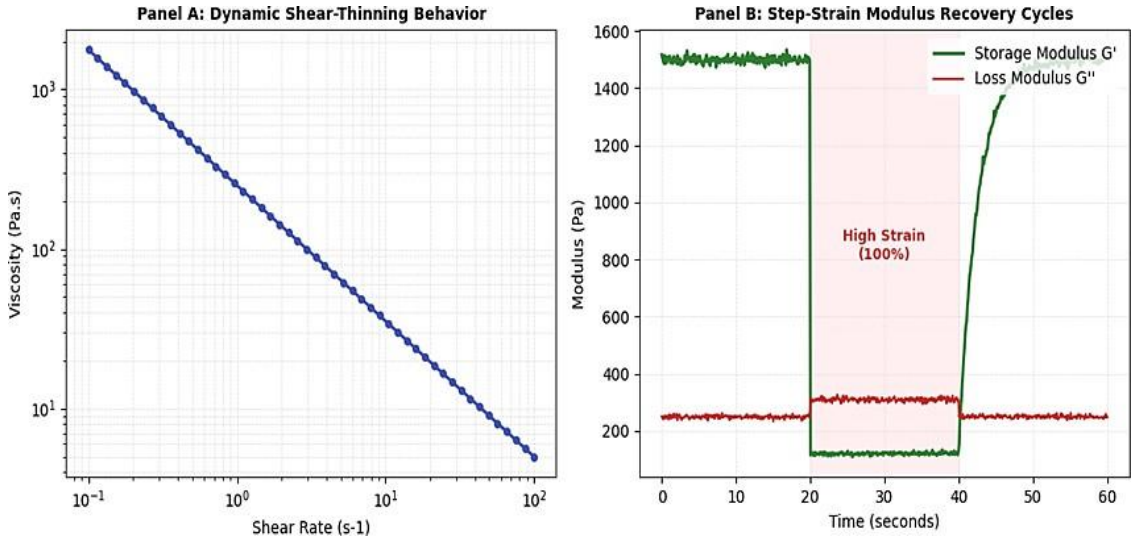

Fig. 4. Viscoelastic and Rheological Properties of the Granular Hydrogel.

under shear. Panel A details the rheological flow curve plotting dynamic viscosity against shear rate from 0.1 to 100 s^{-1}, illustrating a prominent shear-thinning response that supports injectability and ease of processing. Panel B displays the self-healing dynamic step-strain test where alternating low strain of 1% and high strain of 100% are applied, demonstrating that the storage modulus G' recovers more than 90% of its initial magnitude within 10 seconds of high strain removal to verify the rapid network reformation of the microgel assembly.

Fig. 5 indicates the water absorption capacity and the degradation rate of the scaffolds over time. Panel A presents the swelling index of the integrated hybrid scaffold as a percentage over 28 days of incubation in phosphate-buffered saline, illustrating a highly stable hydration profile. Panel B displays the cumulative mass loss percentage of the hybrid scaffold compared with the pure fiber mesh over 28 days, confirming the gradual and controlled degradation of both the hydrogel phase and the polymer fibers.

Rheological testing of the granular hydrogel component revealed a classical shear-thinning response: viscosity decreased by more than three orders of magnitude when the shear rate was increased from 0.1 to 100 s^{-1}. In step-strain self-healing tests, the storage modulus (G') was fully restored within 10 seconds of transitioning from high strain (100%) back to low strain (1%), confirming that the stabilized microgel network can reform efficiently after deformation.

In Vitro Release Profiles of Icaritin

The release kinetics of Icaritin from the hybrid system were evaluated by HPLC. The system exhibited a controlled release profile,

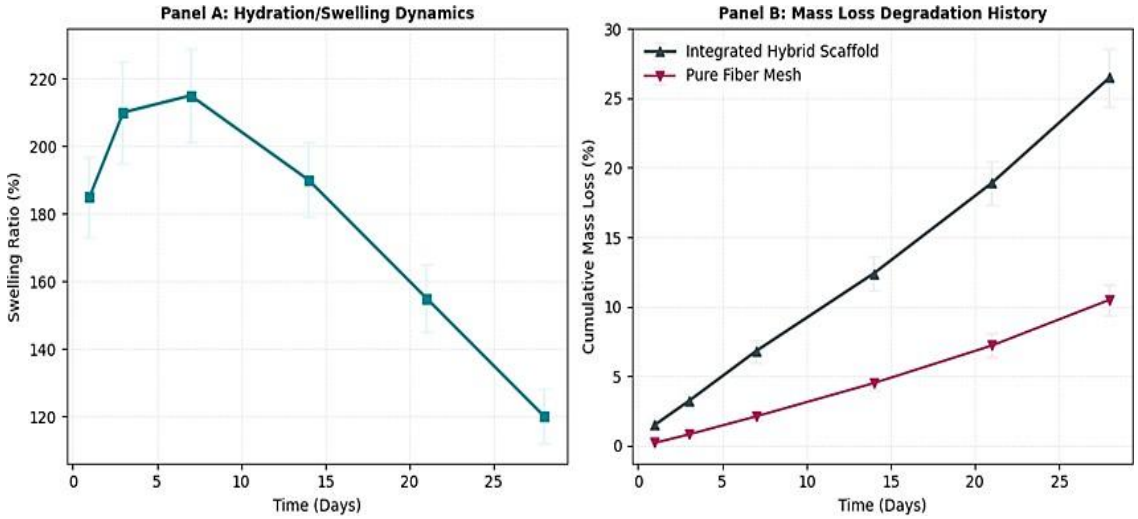

Fig. 5. Swelling Behavior and Biodegradation Profile of the Scaffold.

Table 2. Swelling Ratio and Cumulative Mass Loss over 28 Days in PBS at 37°C.

Timepoint (Days)	Swelling Ratio (%)	Hybrid Scaffold Mass Loss (%)	Pure Fiber Mesh Mass Loss (%)
1	185 +/- 12	1.5 +/- 0.3	0.2 +/- 0.05
3	210 +/- 15	3.2 +/- 0.5	0.8 +/- 0.12
7	215 +/- 14	6.8 +/- 0.8	2.1 +/- 0.35
14	190 +/- 11	12.4 +/- 1.2	4.5 +/- 0.52
21	155 +/- 10	18.9 +/- 1.6	7.2 +/- 0.85
28	120 +/- 8	26.5 +/- 2.1	10.5 +/- 1.10

with approximately 15.2% of the loaded drug released on Day 1 and a steady, sustained release thereafter, reaching 95.6% cumulative release by Day 28. This sustained release is beneficial for maintaining a therapeutic concentration of the drug in the local defect microenvironment over an extended period.

Fig. 6 indicates the anisotropic mechanical behavior and the spatiotemporal release of the encapsulated phytotherapeutic agent. Panel A presents the tensile stress-strain curves of random and aligned meshes alongside the hybrid scaffold tested in both longitudinal and transverse directions, showcasing that the longitudinal hybrid scaffold reaches an ultimate tensile strength of 14.2 +/- 1.1 MPa which is suitable for mimicking the anisotropic mechanical properties of native articular cartilage. Panel B outlines the cumulative in vitro release curve of Icaritin as a percentage over 28 days determined via high-performance liquid chromatography, illustrating a highly sustained and steady release pattern that avoids an initial burst release by releasing approximately 15.2% on the first day and progressing to 95.6% at the end of four weeks.

In Vitro Cell Viability, Alignment, and Multilineage Differentiation

CCK-8 assays confirmed that all scaffold formulations supported BMSC proliferation, with no signs of cytotoxicity. Fluorescence microscopy of F-actin-stained cells demonstrated that BMSCs cultured on the aligned fibers and hybrid scaffolds aligned parallel to the fiber axis within 3

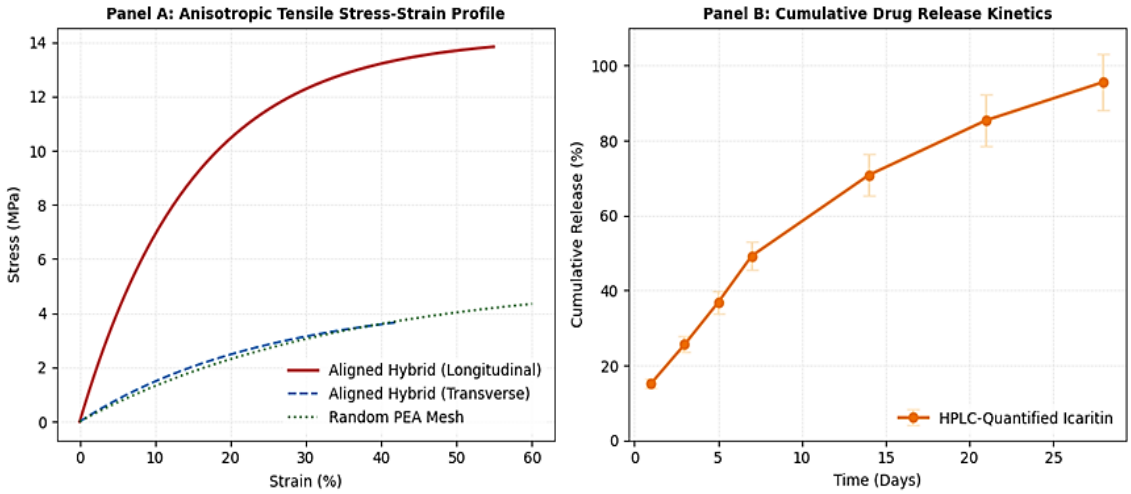

Fig. 6. Mechanical Tensile Performance and HPLC Drug Release Kinetics.

Table 3. Cumulative In Vitro Release of Icaritin from the Integrated Hybrid Scaffold.

Sampling Time (Days)	Concentration of Released Icaritin (μg/mL)	Cumulative Release Percentage (%)
1	3.04 +/- 0.25	15.2 +/- 1.2
3	5.12 +/- 0.42	25.6 +/- 2.1
5	7.36 +/- 0.58	36.8 +/- 2.9
7	9.84 +/- 0.75	49.2 +/- 3.7
14	14.16 +/- 1.10	70.8 +/- 5.5
21	17.08 +/- 1.35	85.4 +/- 6.8
28	19.12 +/- 1.50	95.6 +/- 7.5

days. Furthermore, the hybrid scaffold containing both nHAp and Icaritin significantly upregulated both osteogenic and chondrogenic marker genes in BMSCs, indicating its potential to support multilineage differentiation.

The morphology and position of bone marrow mesenchymal stem cells (MSCs) were determined using fluorescence microscopy which is displayed in Fig. 7. Fluorescence images of MSCs grown on randomly oriented fiber meshes show that their cytoskeletons spread randomly without order as shown in Panel A. When MSCs were cultured on engineered aligned fiber meshes (and hybrid scaffolds), their F-actin cytoskeletons (stained green) aligned along the mesh axis of the fibers and displayed appropriate cytoskeletal guidance as shown in Panel B.

Cells must also proliferate and express lineage-specific genes in order for them to proliferate normally and develop into bone or cartilage when cultured on engineered scaffolds. Cells of the different hybrid scaffold groups show the proliferation of MSCs as demonstrated by the CCK-8 assay (Fig. 8, Panel A) and measured cytokine levels were shown to be approximately equal at all three time points (day 1, day 3 or day 7) which indicated that hybrid scaffolds are cytocompatible and biocompatible. The expression of osteogenic (Runx2 and OCN) and chondrogenic (Collagen II and Aggrecan) gene markers were also quantified for all groups and at both 7 and 14 days post-culture. Every gene was determined to have significantly greater expression in the integrated hybrid group than as compared to the aligned hybrid or random hybrid groups. This indicated that the aligned and integrated hybrid scaffold can direct MSCs to differentiate towards both the osteogenic and chondrogenic lineages.

In Vitro Paracrine Immunomodulation

The potential of the hybrid scaffolds to modulate macrophage activity was assessed by analyzing RAW 264.7 mouse macrophages cultured on either of the hybrid scaffolds and measuring their cytokine secretion. The integrated hybrid scaffold exhibited a significant decrease in the secretion of pro-inflammatory cytokines (TNF-alpha and IL-1beta), while exhibiting statistically significant increases in both anti-inflammatory and pro-healing cytokines (IL-10 and TGF-beta 1), indicating polarization towards an M2 macrophage phenotype.

Fig. 9 indicates the polarization state of host macrophages and their cytokine secretion profile when interacting with the scaffolds. Panel A shows the qPCR gene expression of the M1 marker CD86 and the M2 marker CD206 in RAW 264.7 macrophages, confirming a shift toward the anti-inflammatory M2 phenotype in the hybrid scaffold group. Panel B presents the concentration values

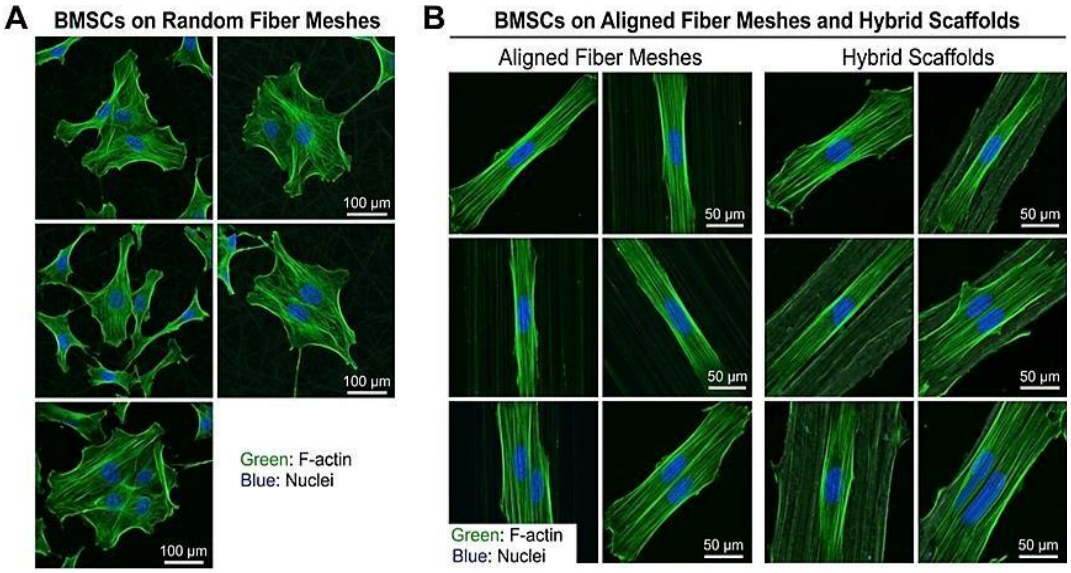

Fig. 7. Cytoskeletal Alignment of BMSCs.

of pro-inflammatory cytokines TNF-alpha and IL-1beta alongside anti-inflammatory cytokines IL-10 and TGF-beta 1 in the culture supernatant measured by ELISA at days 3 and 7, highlighting that the sustained release of Icaritin establishes a pro-regenerative microenvironment by significantly reducing inflammatory signaling and boosting pro-healing factors.

In Vivo Evaluation of Osteochondral Interface Regeneration

At 4 and 12 weeks post-implantation in rabbits micro CT analysis of the subchondral bone compartment (i.e. bone volume fraction (BV/TV) and trabecular thickness (Tb.Th)) showed the hybrid scaffold group had a significantly greater BV/TV and Tb.Th than the other two groups. Smooth, continuous cartilage within the regenerated subchondral bone compartment was confirmed by histological evaluation using Safranin-O staining and Wakitani scores in the hybrid scaffold group.

The results shown in Fig. 10 describe the qualitative micro CT analysis of how subchondral bone has been reconstructed in rabbits at various time intervals. Panel A shows 3D sagittal and transverse micro CT rendering images of

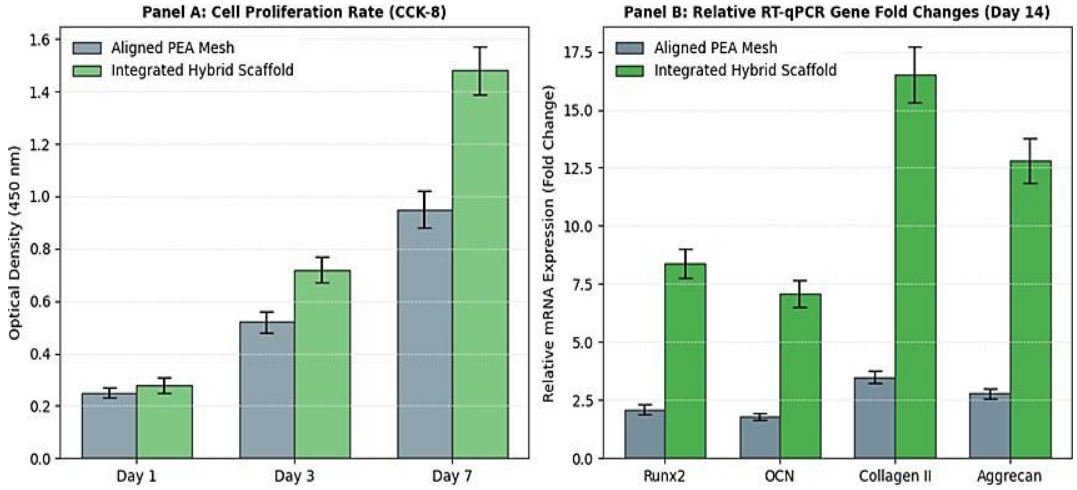

Fig. 8. In Vitro Viability and Osteochondral Gene Expression of BMSCs.

Table 4. Fold-Expression of Target Differentiation Genes in BMSCs at Day 7 and Day 14.

Gene Target	Timepoint	Aligned PEA Mesh	Aligned PEA/nHAp	Integrated Hybrid Scaffold
Runx2 (Osteogenic)	Day 7	1.8 +/- 0.15	3.5 +/- 0.28	5.8 +/- 0.45
	Day 14	2.1 +/- 0.20	4.8 +/- 0.35	8.4 +/- 0.62
OCN (Osteogenic)	Day 7	1.2 +/- 0.10	2.5 +/- 0.18	4.2 +/- 0.35
	Day 14	1.8 +/- 0.14	3.9 +/- 0.32	7.1 +/- 0.58
Collagen II (Chondrogenic)	Day 7	2.2 +/- 0.18	1.5 +/- 0.12	9.2 +/- 0.75
	Day 14	3.5 +/- 0.28	2.1 +/- 0.18	16.5 +/- 1.20
Aggrecan (Chondrogenic)	Day 7	1.9 +/- 0.14	1.3 +/- 0.09	7.9 +/- 0.60
	Day 14	2.8 +/- 0.22	1.9 +/- 0.15	12.8 +/- 0.95

femoral patellar groove defects for each of the three treatment groups – empty control, aligned fiber mesh and hybrid scaffold at the 4 week post-operative time point. Panel B displays the corresponding 3D micro CT rendering images of these same defects at the 12 week time point and demonstrates successful filling and remodelling of the subchondral compartment in the hybrid scaffold treatment group.

The quantitative analysis of the healing of regenerated bone tissue and histological recovery of regenerated bone tissue in the rabbit model is illustrated in Fig. 11. Panel A presents quantitative bar graphs for two measures of newly formed bone (bone volume fraction and trabecular thickness) at 4 and 12 weeks. The hybrid scaffold had the highest bone volume fraction of 74.8 +/- 5.1% at the 12 week time point confirming the superior ability of the hybrid scaffold to induce bone remodelling. Panel B shows Wakitani histopathology scores as quantitative bar graphs at the 4 and 12 week time points confirming that cartilage formed at

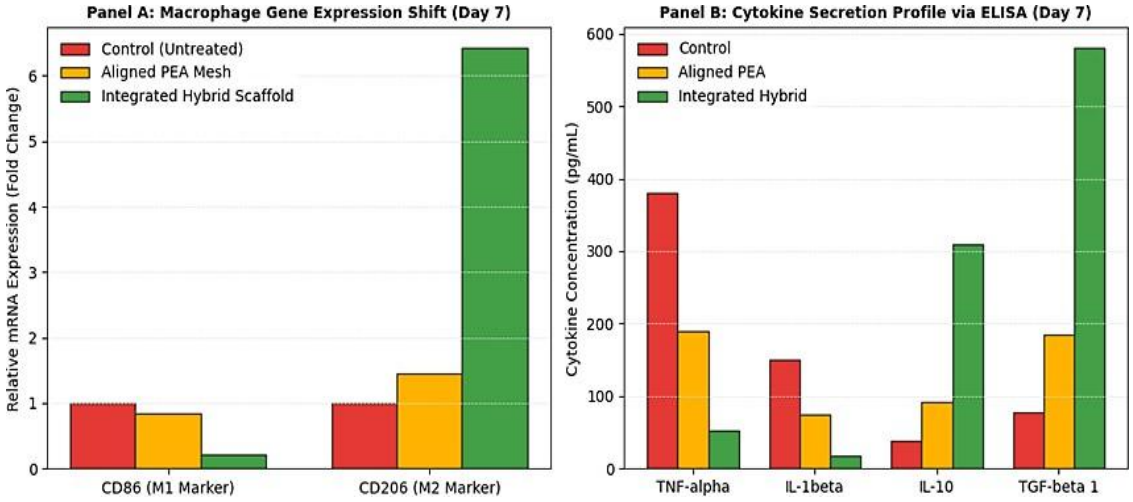

Fig. 9. In Vitro Macrophage Polarization and ELISA Cytokine Profiling.

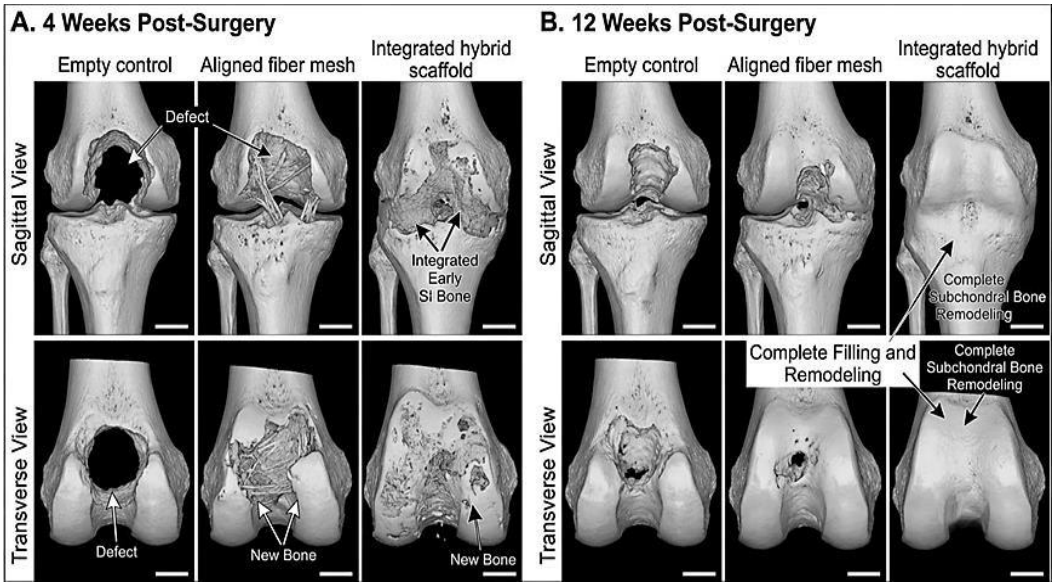

Fig. 10. In Vivo Subchondral Bone Repair via 3D Micro-CT Reconstruction.

the articular interface is of greater quality when regenerated with the hybrid scaffold.

At Week 12, histological analysis of the regenerated tissue demonstrated that defects receiving the hybrid scaffold were filled with a smooth cartilage surface with abundant GAG deposition that blended with the host cartilage. Successful structural integration at the interface was confirmed by immunohistochemical analysis showing strong, localized expression of Collagen Type II in the superficial cartilage layer and that Collagen Type I was expressed only in the newly mineralized subchondral bone zone.

Optical microscopy shows that the repaired osteochondral interface at 12 weeks after surgery is structurally integrated and has a uniform distribution of cartilage to bone in the zonal structure (Fig. 12). The histopathology micrographs of the stained joint sections in each panel with hematoxylin and eosin (overall tissue structure), Masson's trichrome (collagen deposition) and Safranin-O/Fast Green (glycosaminoglycan staining) show a smooth, continuous articular surface, with the hybrid group having thick glycosaminoglycan staining. The immunohistochemical analysis of Collagen Type II, which was localized in the neocartilage layer and Collagen Type I which was localized in the underlying subchondral bone, is shown in Panel B, demonstrating successful reconstruction of a distinct and integrated osteochondral interface.

The regeneration of the osteochondral unit is a challenge in orthopedic research that is complicated by the complex nature of the

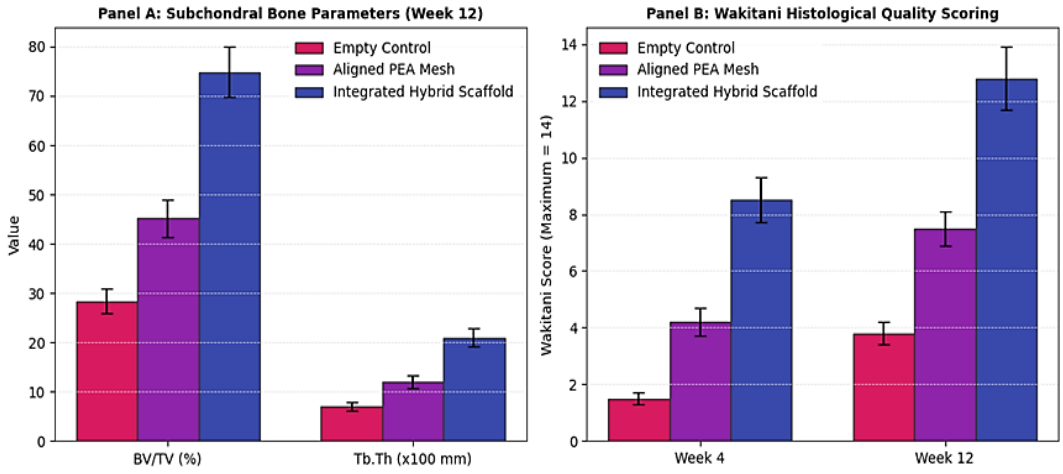

Fig. 11. In Vivo Quantitative Bone Parameters and Histological Scores.

Table 5. Macrophage Cytokine Concentrations (pg/mL) in Culture Supernatant.

Cytokine Measured	Timepoint	Untreated Control	Aligned PEA Mesh	Integrated Hybrid Scaffold
TNF-alpha (M1)	Day 3	450 +/- 35	280 +/- 22	95 +/- 8
IL-1beta (M1)	Day 3	185 +/- 14	110 +/- 10	34 +/- 3
	Day 7	150 +/- 11	75 +/- 6	18 +/- 2
IL-10 (M2)	Day 3	25 +/- 2.2	65 +/- 5.4	195 +/- 15
	Day 7	38 +/- 3.1	92 +/- 7.8	310 +/- 24
TGF-beta 1 (M2)	Day 3	52 +/- 4.5	120 +/- 11	340 +/- 28
	Day 7	78 +/- 6.2	185 +/- 14	580 +/- 42

multitissue unit [1, 2]. The repair needs to be able to support the highly hydrated cartilage layer, which is avascular and a specific subchondral bone plate, which is load-bearing and mineralized [5, 6]. This study focussed on a hybrid biomaterial system composed of aligned electrospun PEA/nHAp fibrous meshes and zwitterionic granular hydrogels, to deliver coordinated physical and biochemical cues [3, 7].

The aligned electrospun fibres showed excellent mechanical properties with a tensile strength of 14.2 +/- 1.1 MPa along the aligned direction in the uniaxial tensile test. This structural organisation is similar to the superficial zone of natural articular cartilage, where the collagen fibrils are parallel to the joint surface, thus resisting tensile and shear forces [10, 16]. Further, the aligned fibers provided contact guidance (physical guidance) cues for elongation and migration of BMSC cells in the fibre direction, known to control

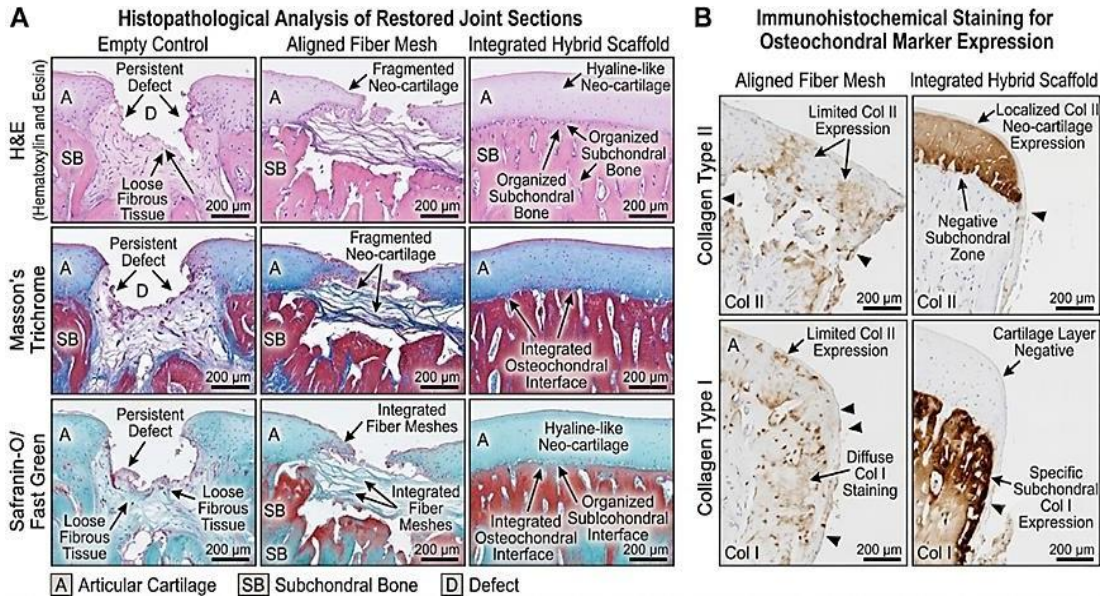

Fig. 12. Histopathological and Immunohistochemical Analysis of the Restored Interface.

Table 6. In Vivo Subchondral Bone Parameters and Wakitani Histopathological Scoring.

Parameters Analyzed	Timepoint	Empty Control Group	Aligned Fiber Group	Integrated Hybrid Scaffold
Bone Volume Fraction (BV/TV %)	Week 4	12.5 +/- 1.4	22.4 +/- 2.1	38.5 +/- 3.2
	Week 12	28.4 +/- 2.5	45.2 +/- 3.8	74.8 +/- 5.1
Trabecular Thickness (Tb.Th, mm)	Week 4	0.04 0.005 +/-	0.06 0.008 +/-	0.11 +/- 0.012
	Week 12	0.07 0.009 +/-	0.12 0.014 +/-	0.21 +/- 0.018
Wakitani Histology Score (Max = 14)	Week 4	1.5 +/- 0.2	4.2 +/- 0.5	8.5 +/- 0.8
	Week 12	3.8 +/- 0.4	7.5 +/- 0.6	12.8 +/- 1.1

cytoskeletal tension and to promote differentiation pathways downstream the fibre direction [14].

A major drawback of dense electrospun fiber meshes, however, is their small pore size, which can prevent the infiltration of cells in three dimensions and diffusion of nutrients [11]. The zwitterionic granular hydrogels were introduced into the fiber network to solve this issue [13]. The granular hydrogels are composed of individual microgel particles that are connected by micro-scale interstitial spaces which enable cell migration and growth inside the construct [14]. Moreover, the zwitterionic SBMA chemistry generates a highly hydrated hydration layer which is non specifically protein-adsorbing [17]. It is thought that this antifouling effect will cause less host foreign body response and prevent fibrotic encapsulation, thus enabling unimpeded cell infiltration and nutrient exchange [12, 17].

Its drug release and immunomodulatory activity are spatiotemporally controlled, which is the key to the biological activity of the hybrid construct [4]. HPLC analysis confirmed a sustained and controlled release of Icaritin over a period of 28 days, which was not the case with monolithic scaffolds previously where a burst release has been observed [15]. This continual release is essential to control the local immune environment [15]. Macrophages are among the initial cells to respond to biomaterials implanted into the body, and the state of polarization of these cells is one of the most important factors that guides tissue healing after their implantation [12].

To evaluate the potential of long-term release of Icaritin, the hybrid scaffold was tested in our in vitro assays, where the production of pro-inflammatory cytokines, such as tumour necrosis factor alpha (TNF-alpha) and Interleukin 1 beta (IL-1beta), was significantly reduced while the production of anti-inflammatory and pro-regenerative cytokines (Interleukin 10 (IL-10) and transforming growth factor beta 1 (TGF-beta 1)) was simultaneously enhanced, suggesting that the sustained release of Icaritin led to a shift in the polarization of RAW 264.7 macrophages from the pro-inflammatory M1 phenotype to the anti-inflammatory and pro-regenerative M2 phenotype. It is hypothesized that secreted factors, such as TGF-beta 1, in this M2-polarized microenvironment will initiate a paracrine signaling cascade that will stimulate migration of local BMSCs and their chondrogenic differentiation [12, 14].

At the same time, the osteoconductive nHAp particles, which formed the core of the fibers, mimicked the mineralized subchondral bone phase [6, 18]. BMSCs exposed to this mineralized phase upregulated some osteogenic marker genes (Runx2, OCN) promoting local matrix mineralization [18]. This dual-differentiation ability was verified by our in vitro results as both chondrogenic markers (Collagen II and Aggrecan) and osteogenic markers (Runx2 and OCN) were significantly increased in BMSCs cultured on the hybrid scaffold.

The therapeutic effect of the hybrid system was also confirmed in vivo in a rabbit osteochondral defect model. At Week 12, defects treated with the hybrid scaffold had very close to complete joint surface restoration with a smooth, hyaline-like cartilage surface with high GAG content and abundant Collagen Type II expression. The subchondral bone plate underneath this superficial layer had a higher BV/TV (74.8 +/-5.1%) and showed high levels of Collagen Type I expression with an orderly trabecular architecture. The lack of a delamination and shear failure commonly seen in non-integrated biomaterials at the interface of the two different tissue layers are ensured by the seamless integration of the two [5, 10]. Based on these findings, the coordinated physical, chemical and immunomodulatory cues provided by this hybrid scaffold system may be useful for the regeneration of functional and integrated osteochondral interface.

CONCLUSION

We created an immunomodulatory hybrid scaffold system for osteochondral interface regeneration with aligned electrospun PEA/nHAp fiber meshes and zwitterionic granular hydrogels in this study. The hybrid constructs showed excellent mechanical properties, hydrophilicity, and self-healing- and shear-thinning properties. It was found that the sustained action of Icaritin was able to induce host macrophages to shift to the anti-inflammatory M2 phenotype in vitro, creating a pro-inflammatory microenvironment. Induced simultaneous osteogenic and chondrogenic differentiation of BMSCs by this paracrine signaling along with the structural alignment of the fibres and osteoconductivity of the nHAp particles. In vivo transplantation was performed in a rabbit model and both functional hyaline-like cartilage and organized subchondral bone was regenerated

in 12 weeks. These findings indicate that this hybrid system has the potential to be a good candidate for osteochondral interface regeneration and joint regeneration.

CONFLICT OF INTEREST

The authors declare that there is no conflict of interests regarding the publication of this manuscript.

REFERENCES

1. Zhou L, Gjvm VO, Malda J, Stoddart MJ, Lai Y, Richards RG, et al. Innovative Tissue-Engineered Strategies for Osteochondral Defect Repair and Regeneration: Current Progress and Challenges. Advanced Healthcare Materials. 2020;9(23).
2. Zhang Y, Han Y, Peng Y, Lei J, Chang F. Bionic biphasic composite scaffolds with osteochondrogenic factors for regeneration of full-thickness osteochondral defects. Biomaterials Science. 2022;10(7):1713-1723.
3. Novotná Rt, Franková J. Materials Suitable for Osteochondral Regeneration. ACS Omega. 2024;9(28):30097-30108.
4. Zhang W, Zha K, Hu W, Xiong Y, Knoedler S, Obed D, et al. Multifunctional hydrogels: advanced therapeutic tools for osteochondral regeneration. Biomaterials Research. 2023;27(1).
5. Whitaker R, Hernaez-Estrada B, Hernandez RM, Santos-Vizcaino E, Spiller KL. Immunomodulatory Biomaterials for Tissue Repair. Chem Rev. 2021;121(18):11305-11335.
6. Bakhshandeh B, Sorboni SG, Ranjbar N, Deyhimfar R, Abtahi MS, Izady M, et al. Mechanotransduction in tissue engineering: Insights into the interaction of stem cells with biomechanical cues. Exp Cell Res. 2023;431(2):113766.
7. Zhong Y, Cao X, Huang M, Lei Y, Liu A-L. Biomimetic bone cartilage scaffolds based on trilayer methacrylated hydroxyapatite/GelMA composites for full-thickness osteochondral regeneration. Int J Biol Macromol. 2025;298:139860.
8. Karami P, Laurent A, Philippe V, Applegate LA, Pioletti DP, Martin R. Cartilage Repair: Promise of Adhesive Orthopedic Hydrogels. Int J Mol Sci. 2024;25(18):9984.
9. Yang Z, Yin G, Sun S, Xu P. Medical applications and prospects of polylactic acid materials. iScience. 2024;27(12):111512.
10. Tong L, Shi G, Liu Q, Qian Z, Li J, Zhang K, et al. Fabrication and evaluation of 3D printed PLGA/nHA/GO scaffold for bone tissue engineering. Sci Rep. 2025;15(1).
11. Li S, Xiaowen Y, Yang Y, Liu L, Sun Y, Liu Y, et al. Osteogenic and anti-inflammatory effect of the multifunctional bionic hydrogel scaffold loaded with aspirin and nano-hydroxyapatite. Frontiers in Bioengineering and Biotechnology. 2023;11.
12. Wang H, Huang R, Bai L, Cai Y, Lei M, Bao C, et al. Extracellular Matrix-Mimetic Immunomodulatory Hydrogel for Accelerating Wound Healing. Advanced Healthcare Materials. 2023;12(27).
13. Bi Z, Cai Y, Shi X, Chen J, Li D, Zhang P, et al. Macrophage-mediated immunomodulation in biomaterial-assisted bone repair: Molecular insights and therapeutic prospects. Chem Eng J. 2024;488:150631.
14. Lei L, Wen Z, Cao M, Zhang H, Ling SK-K, Fu BS-C, et al. The emerging role of Piezo1 in the musculoskeletal system and disease. Theranostics. 2024;14(10):3963-3983.
15. Song Z, Cheng Y, Chen M, Xie X. Macrophage polarization in bone implant repair: A review. Tissue Cell. 2023;82:102112.
16. Levato R, Jungst T, Scheuring RG, Blunk T, Groll J, Malda J. From Shape to Function: The Next Step in Bioprinting. Adv Mater. 2020;32(12).
17. Du J, Zhu Z, Liu J, Bao X, Wang Q, Shi C, et al. 3D-printed gradient scaffolds for osteochondral defects: Current status and perspectives. International Journal of Bioprinting. 2024;9(4):724.
18. Jia Y, Le H, Wang X, Zhang J, Liu Y, Ding J, et al. Double-edged role of mechanical stimuli and underlying mechanisms in cartilage tissue engineering. Frontiers in Bioengineering and Biotechnology. 2023;11.
19. Zhang B, Huang J, Narayan RJ. Gradient scaffolds for osteochondral tissue engineering and regeneration. Journal of Materials Chemistry B. 2020;8(36):8149-8170.
20. Peng Z, Sun H, Bunpetch V, Koh Y, Wen Y, Wu D, et al. The regulation of cartilage extracellular matrix homeostasis in joint cartilage degeneration and regeneration. Biomaterials. 2021;268:120555.
21. Tuerlings M, van Hoolwerff M, Houtman E, Suchiman EHED, Lakenberg N, Mei H, et al. RNA Sequencing Reveals Interacting Key Determinants of Osteoarthritis Acting in Subchondral Bone and Articular Cartilage: Identification of IL11 and CHADL as Attractive Treatment Targets. Arthritis and Rheumatology. 2021;73(5):789-799.
22. Sun Q, Zhen G, Li TP, Guo Q, Li Y, Su W, et al. Parathyroid hormone attenuates osteoarthritis pain by remodeling subchondral bone in mice. eLife. 2021;10.
23. Wu J, Zhang H, Deng R, Xing L, Hu M, Fu X. Interleukin-Iβ promotes cartilage degeneration by regulating forkhead box protein O4 and type Ⅱ collagen. Mol Med Report. 2021;24(5).
24. Wang S, Zhao S, Yu J, Gu Z, Zhang Y. Advances in Translational 3D Printing for Cartilage, Bone, and Osteochondral Tissue Engineering. Small. 2022;18(36).
25. Santos-Beato P, Midha S, Pitsillides AA, Miller A, Torii R, Kalaskar DM. Biofabrication of the osteochondral unit and its applications: Current and future directions for 3D bioprinting. Journal of Tissue Engineering. 2022;13.
26. Chen R, Pye JS, Li J, Little CB, Li JJ. Multiphasic scaffolds for the repair of osteochondral defects: Outcomes of preclinical studies. Bioactive Materials. 2023;27:505-545.
27. Ouyang L, Armstrong JPK, Lin Y, Wojciechowski JP, Lee-Reeves C, Hachim D, et al. Expanding and optimizing 3D bioprinting capabilities using complementary network bioinks. Science Advances. 2020;6(38).
28. Chimene D, Kaunas R, Gaharwar AK. Hydrogel Bioink Reinforcement for Additive Manufacturing: A Focused Review of Emerging Strategies. Adv Mater. 2019;32(1).
29. Taghipour YD, Hokmabad VR, Del Bakhshayesh AR, Asadi N, Salehi R, Nasrabadi HT. The Application of Hydrogels Based on Natural Polymers for Tissue Engineering. Curr Med Chem. 2020;27(16):2658-2680.
30. Neves MI, Moroni L, Barrias CC. Modulating Alginate Hydrogels for Improved Biological Performance as Cellular 3D Microenvironments. Frontiers in Bioengineering and Biotechnology. 2020;8.